Structural and Optical Properties of La_2NiTiO_6 Double Pervoskite

Devesh M. Sirothiya[1,a)], Neha Solanki[2], Netram Kaurav[2], and Ashutosh Mishra[1]

[1]*School of Physics, Vigyan Bhawan, Devi Ahilya University, Indore 452001, India.*
[2]*Department of Physics, Government Holkar Science College, Indore 452001, India.*
[a)]Corresponding author: sirothiya.devesh@gmail.com

Abstract: Among multifunctional $La_2BB'O_6$ (*B*/*B*' are transition metals) with d^6-d^0 nature, double perovskites, La_2NiTiO_6 has recently received significant attention due to its rich physics and prospects in technological applications. In the present study, La_2NiTiO_6 (LNTO) was synthesized via citrate route. The profile analysis of room temperature X-ray diffraction data emphasized on the formation of single phase monoclinic (P21/n) LNTO ceramics. While, in order to optimize the type of band-to-band transition in the synthesized sample, the optical absorbance spectra recorded in the wave length range (200-1100) nm.

INTRODUCTION

The limitation of many existing ferroelectric oxides is a large electronic band gap (ie. 3eV), which is typical of d_0 systems where the gap is between the oxygen 2p and the nominally empty transition metal d states. Band gaps of this magnitude are problematic, as they cannot capture a significant component of the visible spectrum. An additional limitation is the extremely low photo-current observed in most ferroelectric oxides, and this problem was long hindered by a lack of a detailed mechanistic understanding. However, the application of shift current theory has provided significant insight into this phenomenon, and it is apparent that strong polarization and covalence are necessary ingredients for enhancing the photocurrent. [1] Among the structure class $A_2BB'O_6$ called the double pervoskite [2], the La (Lanthanum) based pervoskite oxides of the type $La_2MM'O_6$, have been widely reported for their successful synthesis and characterization in search of the various fruitful physical and chemical properties. Among the various chemical compositions of the pervoskite oxides, the LNTO compound's potential did not studied well experimentally. Hence, there is so much to be discover in accordance with widely reported publications of the global theoretical and computational physicists. Though there are very few publications on the LNTO compound where they have discussed the structural features and few physical and chemical properties of these compounds. They mentioned only few points about their electronic properties and activation energy [3-9] but neither the detailed information was given by them on optical properties of this compound nor the experimental details are published anywhere so far. The theoretical predictions and the lacking of the literature in accordance with the optical property of the LNTO compound motivated us, therefore in the present studies, we have taken up the synthesis, structural and Optical characterization of the system LNTO compound to understand the nature and mechanism of electrical conduction in these materials.

EXPERIMENTAL

LNTO Samples were prepared using the citrate route in order to increase the homogeneity of the starting mixture of the elements. The starting salts were $La(NO_3)_3.6H_2O$ (Alfa Aesar, purity 99.99%), $Ni(NO_3)2.6H_2O$ (Alfa Aesar, 99.99085% metal basis). The raw powders, in stoichiometric ratio, were mixed together in distilled water under constant stirring. Titanium (IV) butoxide (Sigma- Aldrich, 97.0 wt %) was thereafter added to the solution, whereupon a white precipitate of hydrated titanium oxide formed. To this precursor mixture, then a

fixed amount of and anhydrous citric acid in deionised water corresponded to three times the total positive charge of the cations was added to the solution as a complex binder to get a well dispersed mixture of the elements in the precursor gel. The resulting clear solution was kept under constant magnetic stirring at 80ºC for 6 h until a viscous gel formed. The gel was further heated in air to 900^{o} C at a rate of 5^{o} C/min and held at 900 ^{0}C for 2 h in order to burn off the organic parts and to produce fluffy black powders. Black powder was ground into fine powder using a pestle and mortar. The amorphous material thus obtained was pressed and fired in air at 1350 ^{0}C for 24 hours. The phase characterization of these materials was carried out by powder X-ray diffraction technique (Bruker D2 Phaser X-ray diffractometer) with Cu K_{α} radiation having wavelength of 1.54 Å. The scanning was done in the region of 2θ from 10° to 90°. While, in order to optimize the type of band-to-band transition in the synthesized sample, the optical absorbance spectra recorded in the wave length range (200-1100) nm.

RESULT AND DISCUSSION

X-ray Powder Diffraction Analysis

XRD profile for LNTO ceramics [Fig.1] shows a single phase with no impurities. The structural analysis was done using the FULLPROOF software [10] reveals that LNTO compound has a monoclinic P21/n symmetry. Structure image of the LNTO compound are shown in the inset of Fig. 1. The estimated crystallite size using the Sherrer formula (determined by MATCH software) is about ~ 400 nm.

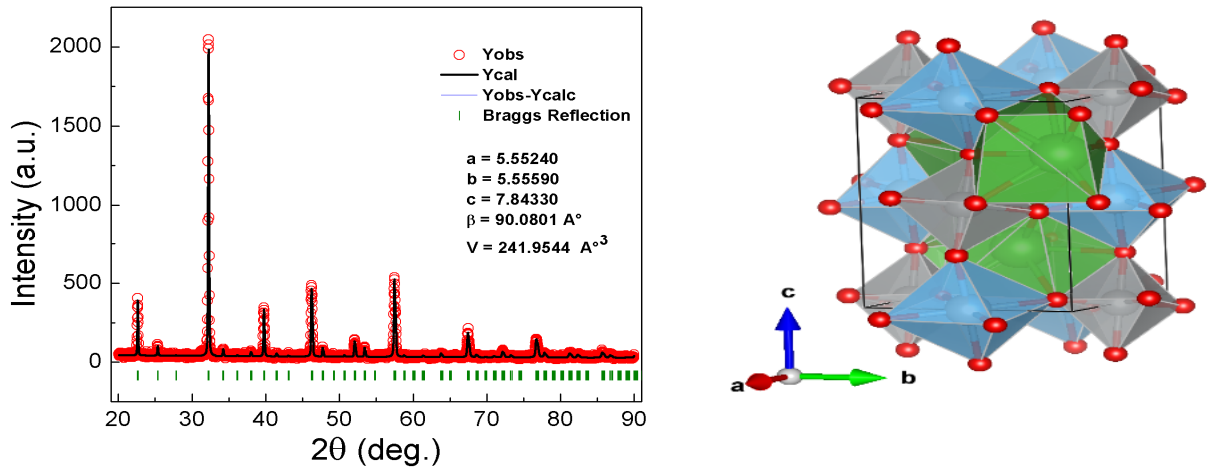

Figure 1. FULLPROOF analysis result of XRD patterns for LNTO compound. The right side figure shows the structure of La2NiTiO6 compound (Image via VESTA software). (Obtained $\chi 2 = 1.09$ with Bragg R-factor: 6.77288 and RF-factor: 10.0819).

UV-Visible Spectroscopy

The LNTO sample has been synthesized by citrate acid precursor method or sol gel method. The absorbance spectra recorded in the wave length (200-1200) nm. In order to optimize the type of band-to-band (for both indirect and direct bandgap for allowed and forbidden) transition in the synthesized sample, it is usual to analyse the optical absorption at the fundamental edge in terms of band-to-band transitions theory [11]. In this treatment, the absorption data follow a power-law behavior of Tauc [12] which is given by:

$$\alpha * h\upsilon = B\,(h\upsilon - Eg)^{n}$$

Where B is an energy-independent constant, hυ is the photon energy, Eg is the optical band gap and assumes values of 'n = 1/2 & 2' for allowed direct, allowed indirect transitions respectively, while 'n = 3 & 3/2' are used for forbidden indirect, and forbidden direct transitions respectively [13]. In order to obtain the Tauc plot to calculate the direct, indirect transitions energy bandgap, the absorption coefficient (α) was calculated from the following equation: $\alpha = 2.303\ A/d$, Where A is absorption and d is the sample thickness.

Figure 2 displays the absorbance *vs* wavelength plot. It shows that the strong absorption bands belong to the *d-d* transitions of molecules from valence band to the conduction band. We have also shown the transmittance with wavelength in inset to the Fig. 2. Fig. 3 shows the α *vs* $h\upsilon$ plot. It can clearly observe that when the absorption coefficient acquires higher values (α >104) cm^{-1} it is expected that direct transition of electron occurs. But, on the other hand whenever the values of absorption coefficient is low (α <104) cm^{-1}, it is expected that indirect transition of electron occur. Apart, there is very little possibility of electron transition at low energy since the energy of the incident photon is not sufficient enough to move the electron from the valance band to the conduction band.

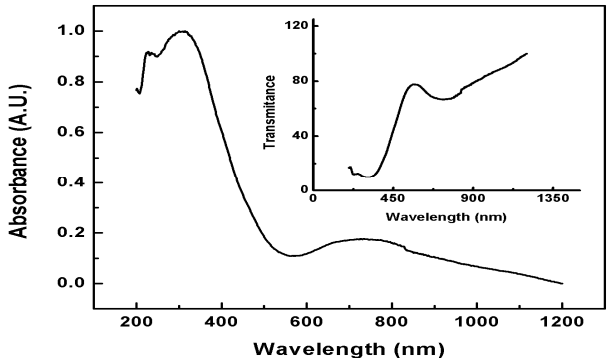

Figure 2. Shows the variation between absorbance with wavelength. Inset: transmittance *vs* wavelength plot.

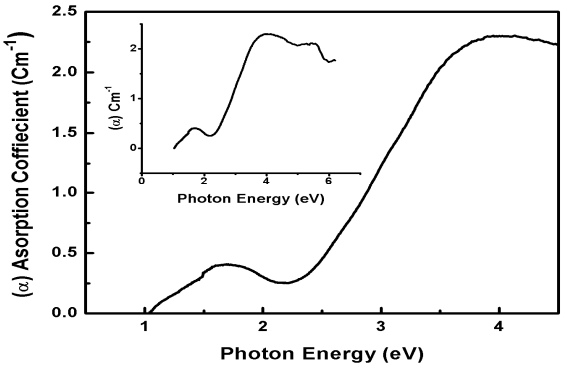

Figure 3. Shows the relation between the absorption coefficient (α) and photon energy ($h\upsilon$). Inset: Shows wider range of (α) *vs* ($h\upsilon$) plot.

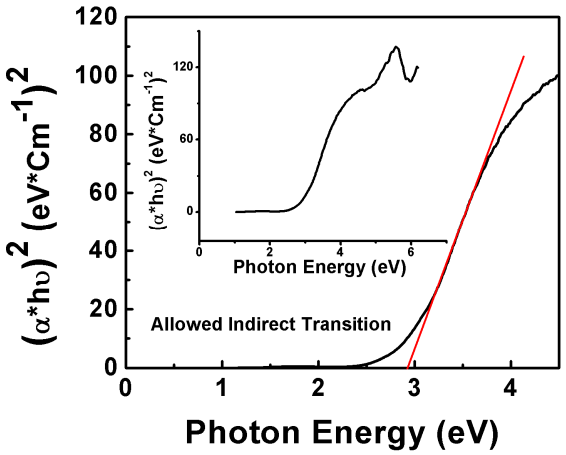

Figure 4. $(\alpha^* h\upsilon)^2$ versus $(h\upsilon)$ plot for an indirect transition. Inset: Shows wider range of $(\alpha^* h\upsilon)^2$ *vs* $(h\upsilon)$ plot

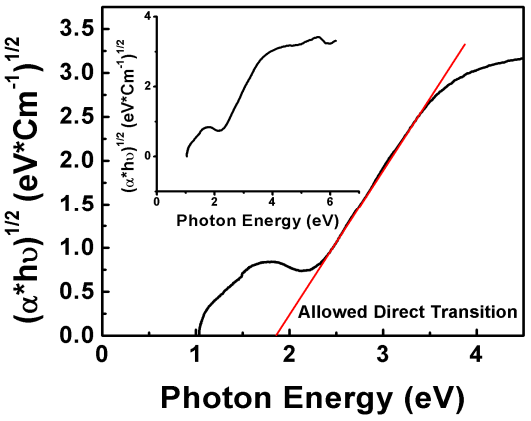

Figure 5. $(\alpha^* h\upsilon)^{1/2}$ versus $(h\upsilon)$ plot for an direct transition. Inset: Shows wider range of $(\alpha^* h\upsilon)^{1/2}$ *vs* $(h\upsilon)$ plot.

Fig.4 shows the $(\alpha^* h\upsilon)^2$ versus $(h\upsilon)$ plot for an indirect transition while, Fig. 5 denotes the $(\alpha^* h\upsilon)^{1/2}$ versus $(h\upsilon)$ plot for direct transition. Here, α is the absorption coefficient and $h\upsilon$ is the photon energy. The photon energy calculated by using the relation $E = (1239/\lambda)$ eV, where λ is the wavelength in nanometers. The value of E $(=h\upsilon)$ extrapolated to $(\alpha^* h\upsilon)$ $n = 0$ gives an absorption energy, which corresponds to a bandgap E_g. Here, $n = 1/2$ used for the calculation of direct bandgap and $n=2$ used to calculate the indirect bandgap.

Figure 6 shows the $(\alpha^* h\upsilon)^{3/2}$ versus $(h\upsilon)$ plot for an direct transition while Fig. 7 denotes the $(\alpha^* h\upsilon)^3$ versus $(h\upsilon)$ plot for direct transition. The value of 'n' used here to estimate the bandgap energy E_g corresponds to the (α*

$h\upsilon$) n = 0 are n=3/2 and n=3. Here, n = 3/2 used for the calculation of direct bandgap and n= 3 used to calculate the indirect bandgap.

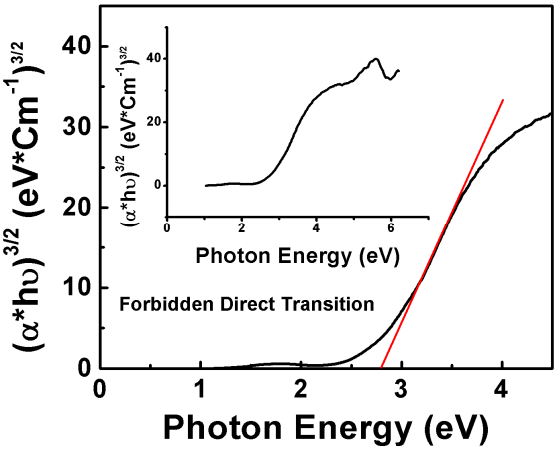

Figure 6. : (α* hυ)$^{3/2}$ versus (hυ) plot for a- forbidden direct transition - bandgap. Inset: Shows wider range of (α* hυ)$^{3/2}$ *vs* (hυ) plot

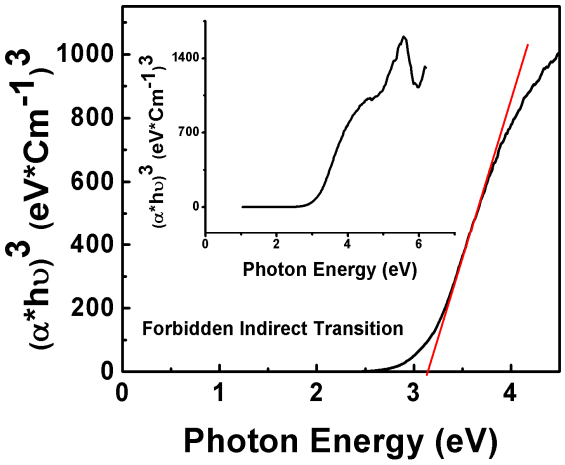

Figure 7. (α* hυ)^{3} versus (hυ) plot for a- forbidden indirect transition - bandgap. Inset: Shows wider range of (α* hυ)^{3} *vs* (hυ) plot.

The resultant value of *Eg* estimated from the (α* hυ) n = 0 (n = 1/2, 1/3, 2/3 & 2) extrapolation for LNTO sample are in form of table 1.

TABLE 1: *Eg* estimated from the (α* hυ) n = 0 (n = 1/2, 1/3, 2/3 & 2) extrapolation for LNTO sample

Transition Type	(α* hυ)^n = 0 ; n	Bandgap - Eg (eV)
Allowed- Direct Transition	1/2	1.66 eV
Allowed – Indirect Transition	2	2.90 eV
Forbidden - Indirect Transition	3	3.12 eV
Forbidden- Direct Transition	3/2	2.78 eV

From the obtained results of the tauc plot, that the direct transition of the electrons from valence band to the conduction band is more dominating in LNTO sample. The reason behind is that for the case of the direct bandgap semiconductors, the electronic transition of the electrons from the valence band to the conduction band is electrical dipole allowed and the both electronic absorption as well as emission therefore dominates usually. While in the case of indirect bandgap semiconductors, electronic transition is electrical dipole forbidden and phonon assisted. Moreover, during the transition process, both the energy and the momentum of the electron–hole pair get changed and which causes weaker absorption and emission as can be understand by obtained results of prepared LNTO sample. Moreover, it is reported that the optical gap energy depends on crystallite size [14], & it increases with decreasing crystallite size in the nano size range. This fact couldn't be verified, since the estimated crystallite size of LNTO sample wasn't in nano size range.

CONCLUSION

To summarize, we have successfully prepared polycrystalline LNTO compound using sol-gel method. The profile matching of the XRD data show that LNTO crystallizes in pure phase monoclinic structure in space group $P2_1/n$. Due to the more efficient absorption of incident energy, direct band gap transitions are dominating with the

E_g = 1.66 eV. The results are encouraging and demands more practical approach towards the LNTO compound for the applications envisaged.

ACKNOWLEDGMENTS

Financial support from the UGC-DAE Consortium for Scientific Research (CSR), Indore under Collaborative Research Scheme is gratefully acknowledged. Authors also would like to acknowledge to Dr. M. Gupta UGC-DAE-CSR, Indore and Dr. Rupesh Devan, IIT, Indore for providing XRD and UV-Vis facilities, respectively.

REFERENCES

1. Chanul Kim, Hyowon Park, and Chris A. Marianetti, Phys. Rev. B **92**, 235122 (2015).
2. E. Rodríguez, M. L. López, J. Campo, M. L. Veiga and C. Pico, J. Mater. Chem. **12**, 2798 (2002).
3. H.R. Fuh, J. Magn. Magn. Mater. (2014).
4. E. Rodreguez, J. Solid State Chem. **148** 479-486 (1999).
5. Pe´rez-Flores JC, Internation, J. Hydrog. Energy (2011).
6. Pe´rez-Flores JC, J. Mater. Chem. **21**, 13195 (2011).
7. Pe´rez-Flores JC, Chem. Mater. **25**, 2484−2494 (2013).
8. N. Ramdass, inaorg, nucl. Chem. **40**, 1453-1454.
9. M. Karolak M. Edelmann and G. Sangiovanni, Cond. Mat. str. el. (2018).
10. M. W. Lufaso and P. M. Woodward, Acta Crystallogr., Sect. B: Struct. Sci. **57**, 725 (2001).
11. M. M. E. Nahass and A. M. Farag, Opt. Laser Technol. **37**, 513–523 (2005).
12. S. Agilan, D. Mangalaraj and S. K. Narayandass, Vacuum **81**, 813–818 (2007).
13. M. M. E Nahass, A. A. M. Farag, E. M. Ibrahim and S. Abd-E-Rahman, Vacuum **72**, 453 (2004).
14. N. Golego, S. A Studenikin and M. Cocivera, Chem. Mater. **10**, 2000 (1998).